Title
Controlling Catalyst—Semiconductor Contacts: Interfacial Charge Separation in p–InP Photocathodes

Journal
ACS Energy Letters, 7(1)

ISSN
2380-8195

Authors
Kaufman, Aaron J
Krivina, Raina A
Shen, Meikun
et al.

Publication Date
2022-01-14

DOI
10.1021/acsenergylett.1c02590

Peer reviewed

ACS Energy LETTERS

http://pubs.acs.org/journal/aelccp

Controlling Catalyst–Semiconductor Contacts: Interfacial Charge Separation in p-InP Photocathodes

Aaron J. Kaufman, Raina A. Krivina, Meikun Shen, and Shannon W. Boettcher*

Cite This: *ACS Energy Lett.* 2022, 7, 541–549

Read Online

ACCESS | Metrics & More | Article Recommendations | Supporting Information

ABSTRACT: **Charge-carrier-selective interfaces between electrocatalyst particles and semiconductor light absorbers are critical for solar photochemistry, but controlling their properties is challenging. Using thin films and nanoparticle arrays of Pt hydrogen-evolution catalysts on p-InP (a high-performance photocathode material), along with macroscopic and nanoscopic electrical and chemical analysis, we show how hydrogen alloying, the pinch-off effect for nanoscale contacts, and the formation of a native surface oxides all play different roles in creating charge-carrier-selective junctions. The new insights can be broadly applied to photocathodes, photoanodes, and overall water-splitting systems to control charge-carrier selectivity and improve performance.**

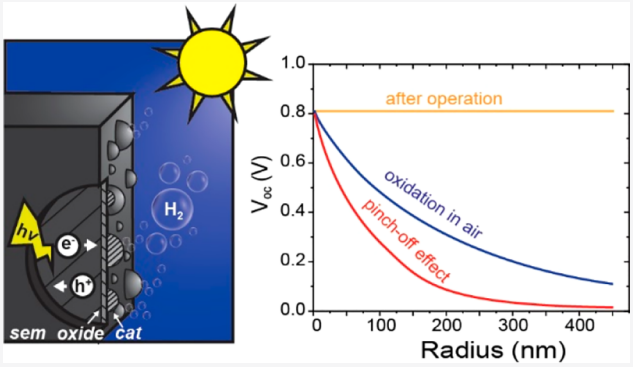

Photoelectrochemical (PEC) water splitting produces H_2 from water and light and offers the possibility of integrating solar-energy conversion with storage, ideally leading to simple lower-cost device architectures. InP is particularly well-suited for efficient conversion of solar to chemical energy because of its ideal bandgap of 1.35 eV, high electron mobility, and low surface-recombination velocity.[1−3] To achieve high efficiency, however, the surface must be coated with electrocatalysts. Pt/p-InP and Pt/p-$Ga_xIn_{1-x}P$, for example, reduce protons with high photocathode efficiency (>12%) and external quantum efficiency (>80%).[1] While Pt is among the most-active for the hydrogen-evolution reaction (HER), Pt also has a high work function (5.65 eV) that is consequently aligned with the Fermi level of p-type InP.[1,4] For example, p-InP with an acceptor concentration of 4×10^{17} cm^{-3} has a Fermi level (5.64 eV) that is more positive than that of Pt (on the vacuum scale), which should form an ohmic, non-carrier-selective contact (i.e., a Schottky barrier of zero) based on conventional theories of metal–semiconductor contacts.[5] However, when this combination is used in photoelectrodes, a rectifying, Schottky-like contact is formed that leads to interfacial photovoltages of >0.7 V and high photocathode efficiencies.[1,3,6] More-recent work has used TiO_2 interlayers to protect the InP, which further appear to increase the interface photovoltage.[7] An improved understanding of the mechanisms for selective collection of photoexcited minority carriers over majority carriers at catalyst/semiconductor interfaces would facilitate the design of durable and efficient photoelectrodes from InP specifically and more generally illustrate design principles that can be translated to other material systems.

There are several possible explanations for the high photocathode efficiencies for p-InP with Pt and other noble-metal catalyst layers. Heller et al. noticed that, for Pt, Ru, or Rh, irrespective of the metal-catalyst work function, the open-circuit voltage (V_{oc}) of the catalyzed photocathode was similar and approached that expected for p-InP contacted with the H^+/H_2 redox couple (0.9 ± 0.2 eV).[1−3] They hypothesized that H_2 permeates the metal catalyst, accumulates at the interface, and sets an interfacial barrier height that leads to high electron selectivity at the H–Pt/p-InP junction (Figure 1a). Aspnes et al. showed in a dry two-electrode system that an H_2 gas atmosphere led to increased rectification of the Pt/p-InP interface, purportedly due to modulation of the Pt work function.[3] Recently, Nunes et al. reported that an interfacial oxide coupled with an H_2 gas atmosphere also yields increased

Received: November 29, 2021
Accepted: December 28, 2021
Published: January 3, 2022

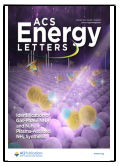

https://doi.org/10.1021/acsenergylett.1c02590
ACS Energy Lett. 2022, 7, 541–549

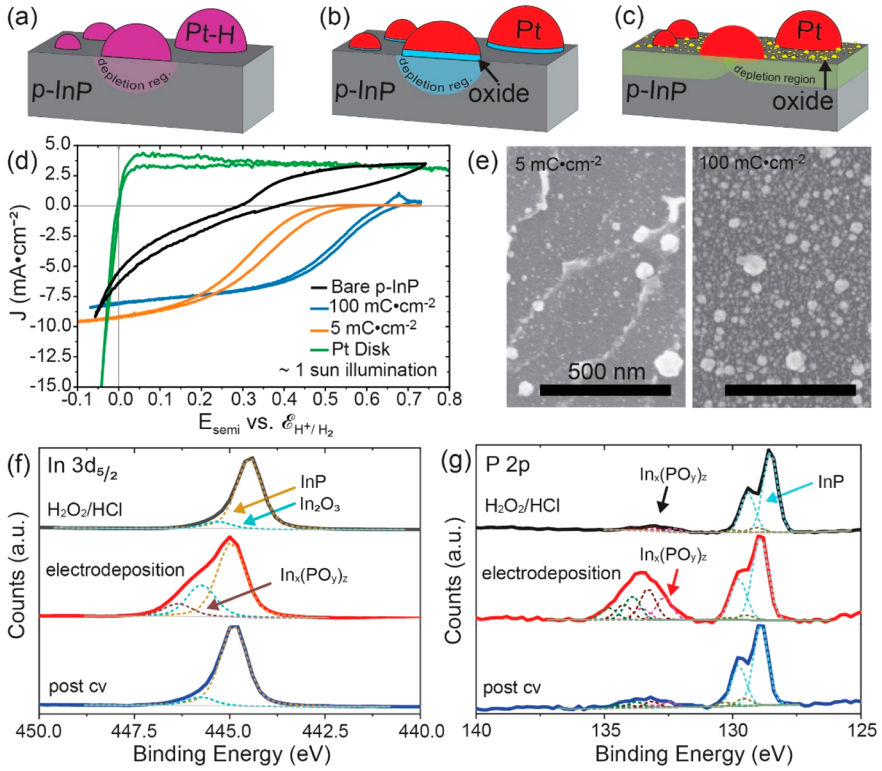

Figure 1. Possible mechanisms of interfacial charge-carrier selectivity in Pt/p-InP photocathodes. (a) Adaptive-junction behavior caused by Pt alloying with H_2 thus lowering its work function. (b) Heterojunction formation by an interfacial oxide. (c) Pinch-off effect caused by a peripheral material increasing the effective barrier at the catalyst/semiconductor interface. (d) Typical photoelectrode *J*–*E* curves in 1 M $HClO_4$ illuminated at ~100 mW cm^{-2} of solar simulation, for two Pt loading conditions (100 and 5 mC cm^{-2} of charge passed during Pt photoelectrodeposition). (e) SEM images of the two samples at the same scale. (f) XPS spectra of the In $3d_{5/2}$ peak show surface conversion of the InP to In_2O_3 from H_2O_2/HCl pretreatment to postelectrodeposition of Pt; the In_2O_3 persists while higher-energy suboxides diminish after illuminated cyclic voltammetry. The shift to higher binding energy of all of the In species is thought to originate from surface-charging effects, as the Pt 4f peaks did not shift. Changes in band bending may also play a role in the shift. (g) Phosphate species of mixed ratios seen near 133 eV in the P 2p spectra were most prevalent after electrodeposition and persist in greater amounts than after etching pretreatment.

electronic barriers/photovoltages in the "theoretically" ohmic Pt/p-Si system.[8]

A second mechanism that could modulate the catalyst/semiconductor interface is the formation of an interfacial oxide (Figure 1b). InP naturally forms a surface oxide consisting of $In_x(PO_3)_z$, $In(PO_4)$, P_2O_5, and In_2O_3 when exposed to air and/or aqueous solution under anodic conditions.[6,9−15] In_2O_3 is typically a conductive n-type oxide; however, it is soluble at the low pH used in electrolytes for these InP photocathodes. This complex oxide may grow directly on p-InP and undercut the Pt particles or form through thin catalyst films *via* oxygen diffusion at defects or pinholes. This n-type oxide could generate an electron-selective contact due to the high conductivity of electrons (over holes) as discussed by Würfel broadly in the context of photovoltaic devices.[16] Such an interlayer might govern the nature of the junction irrespective of the metal-catalyst deposited on the upmost layer. The construction of n-In_2O_3/p-InP heterojunction solid-state solar cells, for example, is known.[17]

The nanoscale size of the metal-catalyst contacts to the p-InP could also be important (Figure 1c). Nanoparticle layers usually result from the photoelectrodeposition of metals on semiconductor surfaces and are often intentionally sought to reduce parasitic optical absorption in the catalyst layer. We previously showed that for Ni nanoparticles contacting n-Si photoanodes, smaller particles give rise to dramatically larger photovoltages and photoelectrode efficiency.[18] This observation was quantitatively explained by the pinch-off effect for heterogeneous nonuniform Schottky contacts. When the radius of nanoscale contacts is similar in dimension to the depletion-region depth in the regions surrounding the nanoscale contacts, a new effective barrier describes the transport through the contact.[18−21] This effective barrier may be modeled analytically by Tung's patch theory to predict a photovoltage that depends on metal nanocontact (catalyst particle) radius (see the Supporting Information).[19]

Herein, we use a combination of macroscale photoelectrode measurements, surface-sensitive spectroscopies, conducting atomic force microscopy (C-AFM), and transmission electron microscopy (TEM), on both well-defined nanopatterned Pt and heterogeneous electrodeposited Pt on p-InP, to illustrate the roles the physical phenomena outlined above play in controlling the charge-carrier selectivity at the catalyzed photochemical junction. Specifically, we discover that hydrogen adsorption/alloying with Pt catalyst material alone is insufficient to explain the large photovoltages at the Pt/p-InP interface, in contradiction to earlier findings. Instead, the formation of an n-type In-rich oxide between the Pt and p-InP appears essential to generate an interface that selectively collects electrons over holes. We further find that the pinch-off effect is indeed critical in setting the interface selectivity at Pt nanoparticles on p-InP prior to the formation of an interface oxide, but that after photochemical testing is not significantly important. These results are useful because they illustrate how

https://doi.org/10.1021/acsenergylett.1c02590
ACS Energy Lett. 2022, 7, 541−549

to engineer interfaces between active catalyst materials and semiconductor absorbers independent of the specific work function of the catalyst and in ways not easily predicted based on traditional Schottky-contact theory. These insights are relevant not only to designing higher-efficiency III−V photocathodes from InP and $Ga_xIn_{1-x}P$ materials but also for more complicated systems like oxide photocatalyst particles where precise control over doping and materials composition is not possible.[7,22−26]

Interface Selectivity. All PEC devices must generate a gradient in the electrochemical potential of electrons ($\nabla\bar{\mu}_n$) and holes ($\nabla\bar{\mu}_p$) to separate and collect photogenerated carriers. This can be realized by different relative electron and hole conductivities at the two contacts to the semiconductor absorber. In a typical photoelectrode, the catalyst surface layer or particles must comprise one selective contact, while the electrical back contact comprises the other. Alternatively, in a dispersed photocatalyst particle that drives both cathodic and anodic reactions on the same absorber, two different, and spatially separated, catalyst sites must yield independent hole- and electron-selective contacts. The profiles in $\bar{\mu}_n$ and $\bar{\mu}_p$ are parameters, however, which one cannot readily engineer. Instead, the relative electron and hole conductivities at each contact are usually controlled with a heterojunction or *via* band bending that depletes the majority carrier.[16] The local electron or hole currents j_n or j_p at a contact are related to the local conductivities σ_n and σ_p and $\nabla\bar{\mu}_n$ and $\nabla\bar{\mu}_p$.

$$j_n = \frac{\sigma_n}{q}\nabla\bar{\mu}_n \tag{1}$$

$$j_p = \frac{-\sigma_p}{q}\nabla\bar{\mu}_p \tag{2}$$

These physics similarly control the performance of contacts in photovoltaic devices. Lonergan and co-workers described selective contacts under open-circuit conditions and determined the limits of photovoltage between the two contacts, V_{oc}. In the context of a photoelectrode, V_{oc} is the steady-state voltage that develops under illumination between the catalyst layer (usually collecting minority carriers) and the back contact to the semiconductor. Lonergan defines the selectivity, S, as the ratio in partial equilibrium-exchange current densities at the respective contact, denoted $\boldsymbol{J_0}$ and j_0 for the dominate and secondary carrier at the semiconductor/contact interface.[27]

$$V_{oc} = \frac{k_bT}{q}\ln(S), \qquad S = \frac{\boldsymbol{J_0}}{j_0} \tag{3}$$

A key fundamental challenge in semiconductor photoelectrochemistry, therefore, is to achieve control over the catalyst/semiconductor contact selectivity to allow for the generation of high photovoltages and photocurrents.

Interface Measurements. Figure 1d shows conventional (macroscopic) photoelectrochemical analysis of p-InP photocathodes coated with electrodeposited Pt nanoparticles (SEM micrographs in Figure 1e). The data show that the Pt particles on p-InP selectively collect photoexcited electrons because the photovoltage is substantial (~0.7 V), and significant photocurrents attributed to HER on the Pt particle surface are measured (~10 mA cm^{-2}). To explore the factors affecting this electron collection, we compare two different Pt loadings photoelectrodeposited with 100 and 5 mC cm^{-2} of integrated cathodic charge passed during Pt deposition from a chloroplatinic acid solution (after an H_2O_2/HCl etch to remove surface oxides). While the V_{oc} and photocurrents for the two samples are similar (Figure 1d, blue and orange curves), the slope of the $J-E$ curves near the open-circuit potential are different. For the sample with 100 mC cm^{-2} of Pt deposition charge, the $J-E$ curve approaches the open-circuit potential near 0.7 V vs the reversible hydrogen electrode (RHE) with a steep slope. In contrast, the $J-E$ curve for the 5 mC cm^{-2} has a shallow slope near V_{oc} suggestive of a tunnel barrier between the Pt and p-InP that is impeding charge transport.[28] The higher density of electrodeposited Pt for the 100 mC cm^{-2} sample apparently reduces the effect of this tunnel barrier. To understand this in more detail, it is necessary to uncover the chemical composition of the interfaces, particularly after photoelectrochemical cycling.[6,24]

Ex situ X-ray photoelectron spectroscopy (XPS) of the p-InP photocathode was used to analyze the surface composition. A control p-InP sample pretreated with H_2O_2/HCl yields a clean InP peak in the In $3d_{5/2}$ peak (Figure 1f) and the P 2p (Figure 1g) spectrum with the absence of significant surface oxide that was present in the as-received sample (Figure S1). After H_2O_2/HCl treatment and the electrodeposition of 5 mC cm^{-2} of Pt, an increase in binding energy for the InP peak in the In $3d_{5/2}$ spectra is observed which agrees with literature values for In_2O_3.[9−11] A mixed indium phosphate peak at higher binding energies is found in the P 2p spectra. Following 1 dark and 5 illuminated CV cycles in 1 M $HClO_4$, the In_2O_3 peak remains but the relative intensity of the mixed indium-phosphate peak decreased (see the discussion of peak position and chemical analysis in the Supporting Information). The presence of a mixed In_2O_3 and $In_x(PO_y)_z$ on InP has been observed previously.[6,10−14] The presence of this mixed oxide observed by XPS coincides with carrier-selective junction behavior we find in the macroscopic photoelectrode $J-E$ curves (Figure 1d).

To study the effects of ambient H_2 on the electrical characteristics of the junction, a 40 nm Pt film was deposited by electron-beam deposition on the p-InP. The creation of a Pt−H interfacial dipole (Figure 2a) formed by the dissociation and diffusion of protons to the Pt(film)/p-InP interface, as in metal/insulator/semiconductor gas-sensor devices, could lower the apparent work function and develop an energetic barrier for holes.[29−31] The nonlinear $J-V$ curves in Figure 2b show that the H_2 indeed induces a small barrier at the Pt(film)/p-InP junction, but the overall $J-V$ characteristics remained nearly symmetric. The developed barrier was reversibly eliminated after the junction was reintroduced to an O_2-containing atmosphere. The absorption of H_2, and the hypothesized Pt work function lowering implied by Figures 2b and 3c, is consistent with the H_2 gas sensor literature.[29−31] However, this mechanism was not observed to transition the pristine Pt(film)/p-InP ohmic junction to a rectifying, electron-selective contact observed in the *operando* data shown in Figure 1d (Pt particles) and Figure 3c (Pt film).[29,30]

The dual-working-electrode (DWE) PEC configuration was then used to study the *operando* Pt/p-InP junction behavior. Figure 3a illustrates the hypothesized Schottky-like junction formed between Pt and p-InP and how the electrode potentials are sensed and controlled. With DWE PEC the applied potential between semiconductor back contact and catalyst, V_{app}, can be controlled and measured directly. We measure the current across the Pt(film)/p-InP junction while simultaneously poising V_{cat} (i.e. E_{cat}/q) at various potentials versus the

https://doi.org/10.1021/acsenergylett.1c02590
ACS Energy Lett. 2022, 7, 541−549

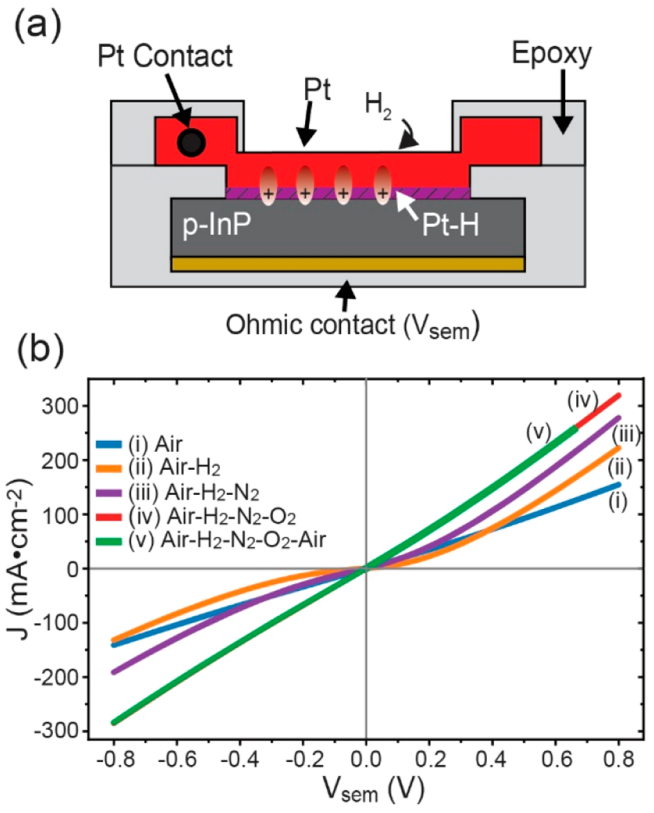

Figure 2. Effect of H_2 on Pt/p-InP interface. (a) Device geometry with top contact to the Pt thin film illustrating one possible mechanism for the formation of electron-selective contacts. H_2 reacts with the Pt thin film to form Pt−H which affects the dipole at the Pt/p-InP interface. (b) Results of dry, macroscopic, two-electrode $J-V$ curves of contacts made by depositing 40 nm of Pt by electron-beam deposition on p-InP (pretreated with conc. HCl) that display ohmic behavior. After treatment with H_2 for 10 min (curve ii), the response deviates from linearity, but no large barrier is apparent. Exposure to an oxidizing O_2/air atmosphere returns the linear $J-V$ response, consistent with loss of absorbed hydrogen.

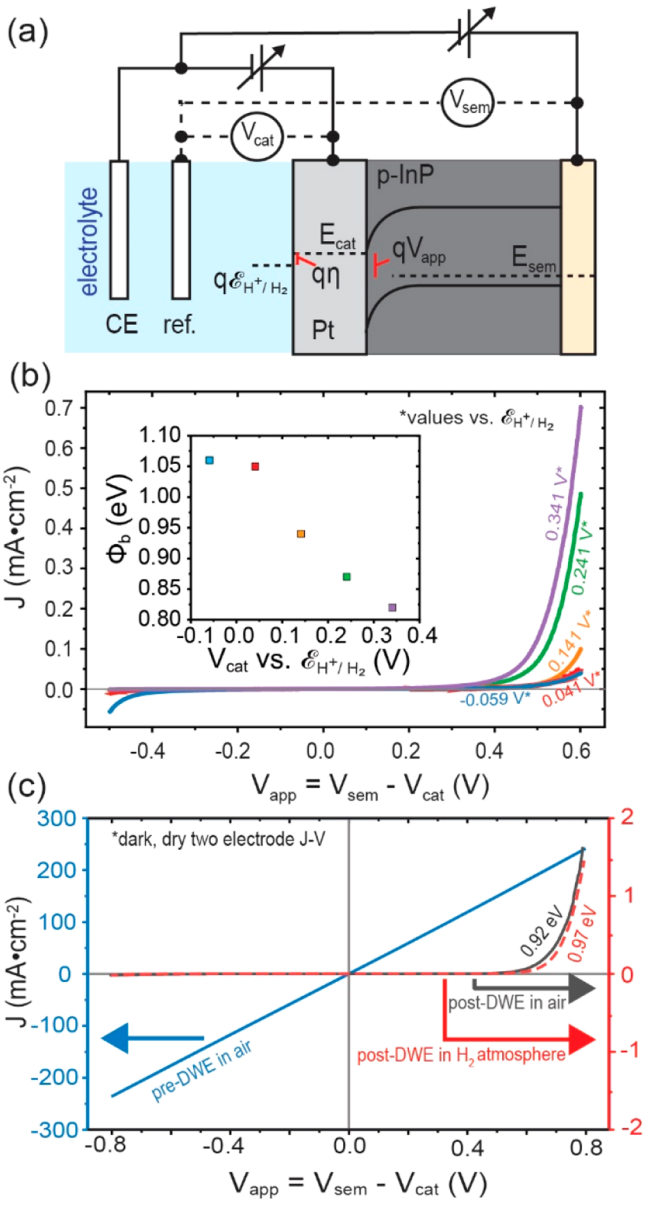

Figure 3. *Operando* dual-working-electrode experiments. (a) DWE PEC experiment schematic. (b) $J-V_{app}$ response as V_{cat} (E_{cat}/q) is controlled relative to a reference electrode (the values of V_{cat} for each curve are labeled next to each versus RHE). The inset plots the calculated barrier height from the Schottky diode equation with respect to V_{cat}. $J-V$ curves shift positive at V_{cat} values approaching 0 V vs. RHE, indicative of the barrier height increase with decreasing V_{cat} evident in the inset. (c) Dry two-electrode measurements before and after the DWE experiment illustrate an irreversible shift from ohmic to rectifying. The apparent Schottky barrier heights from fitting the $J-V$ curves are printed next to each curve.

reference electrode in the electrolyte. The $J-V_{app}$ characteristics of the junction were rectifying under *operando* conditions, which is different than the ohmic behavior observed *ex situ*. As discussed below, we propose an interfacial oxide layer grows by diffusing to the interface through the Pt film. This interfacial oxide likely dictates the junction properties.

The irreversible change observed in the $J-V$ curves after the DWE experiment in Figure 3c contrasts the reversible Pt work-function lowering caused by H_2 absorption in Figure 2b and suggests a permanent transition, like that of Pt/p-InP converting to a Pt/InO_x/p-InP heterojunction. Additionally, the measured current in Figure 3c was nearly 2 orders of magnitude lower after DWE PEC experiments than before, indicating a more resistive junction. V_{cat} was stepped from 0.241 V to −0.059 V then stepped back to 0.341 V vs RHE in 1 V increments. Calculated from the Schottky diode equation, barrier heights in Figure 3b increased systematically with more-negative V_{cat} indicative of a degree of adaptive-junction behavior, but they level off at V_{cat} more negative than the RHE.[18,32,33] The largest barrier heights, >1 eV, are similar to those observed in In_2O_3/p-InP heterojunctions.[17] At V_{cat} positive of RHE, the barrier height of the interfacial oxide linearly tracked with V_{cat}, probably due to electrochemical doping of the newly formed interfacial oxide. More negative V_{cat} would be expected to increase its Fermi level as the oxide is reduced and charge-compensating protons intercalated, leading to the observed adaptive-junction behavior.[34−38] We propose the constant barrier height observed at potentials near, and more negative than, the RHE is fixed by the redox potential of H^+/H_2.[1] At more-negative potentials than the RHE the Pt catalyst and InO_x is fixed at the redox potential of H^+/H_2, and the remaining voltage is dropped in the double

https://doi.org/10.1021/acsenergylett.1c02590
ACS Energy Lett. 2022, 7, 541−549

layer of the electrolyte rather than in the oxide. The calculated barrier height was observed to reversibly decrease when qV_{cat} was returned positive to 0.341 V vs RHE. While the small change in barrier height (Δ = 0.24 eV in Figure 3b inset) was observed to be reversible from qV_{cat} −0.059 to 0.341 V vs RHE under electrochemical conditions, the dry $J-V$ characteristics were not reversible from before to after the DWE experiment (Figure 3c) (*i.e.*, which changed from ohmic to rectifying). After the *operando* DWE measurements, the dry junction was still sensitive to H_2 gas with a calculated barrier height increase of 0.05 eV under H_2. This was, however, a factor of 5 smaller change than the increase during electrochemical reduction of protons.

As opposed to the thin-film Pt catalyst layers described above, most photoelectrodes use nanoparticle catalysts to decrease parasitic light absorption. Catalyst nanocontacts, however, often display differing electrical properties than their thin-film analogues.[18] Dry, conducting AFM (C-AFM) was thus used to measure the electrical-transport properties across individual Pt nanocontacts. Semiconductor photoelectrodes are usually decorated with electrocatalyst particles by electrodeposition.[1,22] By controlling the integrated cathodic charge during photoelectrodeposition, we produced a range of Pt particle densities (Figure S7). The 5 mC cm^{-2} samples were used for their low particle densities with a variety of diameters which could be independently measured by C-AFM on a single electrode (Figure S7). $J-V$ curves from electrodeposited Pt particles displayed a barrier of 0.86 ± 0.16 eV independent of particle size (Figure S8). The InP surface for these samples also contained substantial In_2O_3 and $InPO_x$ (based on XPS analysis) after electrodeposition.

To assess the role of nanocontacts in the absence of substantial interfacial oxide, we then studied Pt nanoparticles on p-InP defined by electron-beam lithography (EBL). Surface oxides were removed by H_2O_2/HCl etching, and nanodisk arrays were created by EBL. Immediately following preparation, the nanocontacts were analyzed by C-AFM and illuminated C-AFM (Figure 4a). The largest disk, approximately 250 nm in radius, displayed nearly ohmic current−voltage ($J-V$) response with a small photovoltage (0.05 V). The smallest disk, approximately 50 nm, displayed a Schottky-like $J-V$ response with a larger photovoltage (0.48 V). The inverse trend of photovoltage with disk radii is exemplified across many contacts and samples in Figure 4b. The same sample was subject to further oxidation in humid, room-temperature air and reanalyzed by illuminated C-AFM. A similar trend in photovoltage was observed with an increase in photovoltage at all radii. The dependence of V_{oc} on particle radius was not observed on EBL-defined nanodisks after being subject to dark and light CV in 1 M $HClO_4$, but rather a roughly constant V_{oc} at all radii was observed.

The Role of Pinch-off. The increased carrier selectivity for the EBL contacts with decreasing radius is readily explained with pinch-off theory.[18] Pt nanodisks (particles), when surrounded by a high-barrier-forming oxide, will begin to adopt the barrier of the peripheral material when their dimension is on the order of, or smaller than, the width of the depletion width in the semiconductor. The pinched-off particles' photovoltage is thus also a function of its radius (see the Supporting Information for further discussion and derivations). When the diameter of the contact is on the order of the depletion region, ~500 nm for the In_2O_3/p-InP junction, the pinch-off effect is expected.[21] Larger Pt/InP

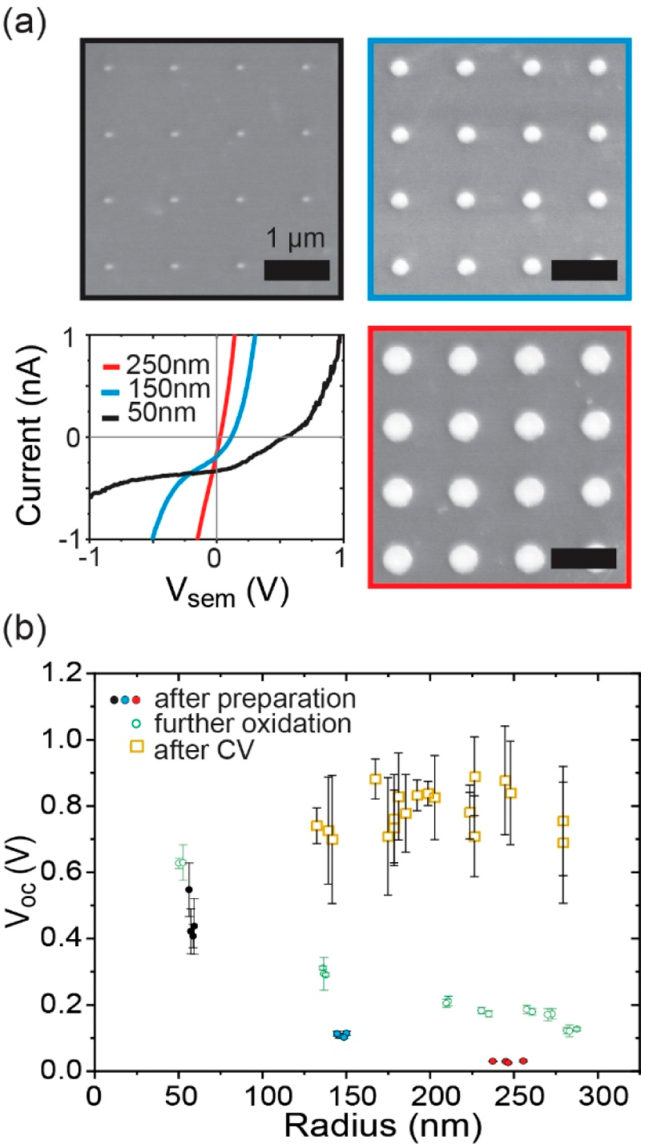

Figure 4. The pinch-off effect measured by C-AFM. Pt nanocontacts, 8 nm thick, deposited on H_2O_2/HCl pretreated p-InP surface by electron-beam lithography, metal evaporation, and lift-off. (a) Representative scanning-electron microscope (SEM) images (top left, top right, bottom right) color-coordinated to $J-V$ curves of individual nanocontacts of corresponding radius from illuminated (~5 suns) conducting AFM (bottom left). (b) The V_{oc} values for Pt/p-InP individual nanocontacts illuminated by laser-light spillover around the probe cantilever extracted from $J-V$ curves. The V_{oc} increases with decreasing nanocontact radius, in agreement with the pinch-off model. The V_{oc} data were collected from the same sample subject to 2 weeks of further oxidation in room-temperature air. Increased V_{oc} was observed for all disk radii. The yellow squares signify V_{oc}'s recorded from a unique sample after a single dark CV (−0.3 to 0.5 V vs SCE) in 1 M $HClO_4$ and 5 illuminated CV cycles (−0.3 to 0.6 V vs SCE), with one-sun equivalent illumination.

nanocontacts (which have not been further oxidized) appear ohmic and are less electron-selective (Figure 4). In fact, even for particles 150 nm in radius, only a small photovoltage is observed, consistent with pinch-off theory that predicts minimal effect as the contact diameter approaches 500 nm in this case. These data support the presence of a thin layer of In_2O_3 natively grown on the peripheral p-InP exposed to air

https://doi.org/10.1021/acsenergylett.1c02590
ACS Energy Lett. 2022, 7, 541−549

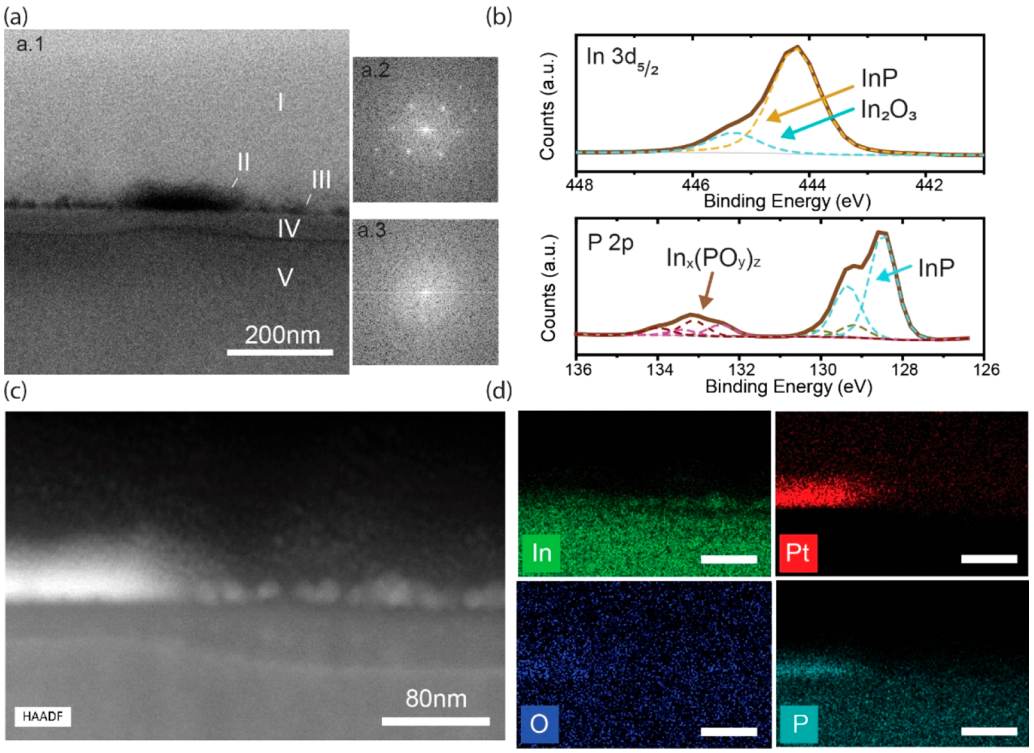

Figure 5. Structural and chemical analysis of nanocontacts following photoelectrochemistry. (a) TEM micrograph of an EBL-defined nanocontact post electrochemistry (a.1) with reduced fast Fourier transforms of region V (a.2) and region IV (a.3). (b) Of the same sample, XPS spectra of In $3d_{5/2}$ (top) and P 2p (bottom) indicate the composition of the sample's surface. (c) High-angle annular dark-field (HAADF) image with correlated EDS maps (d) of In (top left), Pt (top right), O (bottom left), and P (bottom right).

following the metal lift-off procedure. Further oxidation in air and by cyclic voltammetry eliminates the pinch-off effect because the particles become undercut by the peripheral oxide (or an interfacial oxide forms by the diffusion of oxygen to the interface through the thin Pt disk) as in Figure 3. Therefore, while the pinch-off effect substantially affects nanoscale contacts between Pt and bare p-InP, it does not appear to be of significant importance in the photochemical devices, unlike Ni/n-Si contacts where it was found to be the dominant effect controlling the interface charge-carrier selectivity.[18]

The Role of Oxide Heterojunctions. A sufficiently thick n-type oxide interlayer, such as In_2O_3, would be expected to form a heterojunction with p-InP.[17] The complex mixed oxide on the surface of p-InP contains In_2O_3 based on XPS (Figures 1 and 5), which has been observed by others under various preparation methods.[6,10,11,13,14] On Pt junctions prepared by electrodeposition, the presence of the mixed oxide was observed directly after deposition and electrochemistry (Figure 1). Because the electrodeposited particles in Figure 1 are all smaller than 80 nm, the particles would be subject to the pinch-off effect as seen in Figure 4b, although no dependence of the particles' radius on its barrier height was observed in Figure S8. The EBL samples, with the surface oxide removed before Pt deposition, also display an interfacial oxide after CV by TEM analysis (Figure 5). Therefore, whether Pt is electrodeposited or deposited by physical vapor deposition (both thin-film and EBL nanocontacts), an interfacial oxide is generated after illuminated electrochemical cycling in 1 M $HClO_4$. The initially pinched-off smallest EBL Pt nanocontacts, while electron-selective, can achieve greater photovoltages by reducing the recombining hole current (j_0) *via* the formation of the surface oxide that is highly electron-conducting (thus increasing selectivity).[16,27]

A TEM cross section of the photoelectrochemically cycled EBL-defined Pt nanodisks further demonstrates the formation of the heterojunction. Cross sections of electrochemically cycled EBL Pt nanodisks reveal an interlayer between the Pt disk and the p-InP substrate (Figure 5a). This interlayer is observed to be amorphous by TEM analysis (Figure 5a.3) and thinner under the Pt disk. Energy-dispersive X-ray spectroscopy (EDS) mapping (Figure 5c,d) displays In in lower concentrations in the interlayer than in the substrate and in higher concentrations in the nodes atop the interlayer next to the Pt disks. In^{3+} may have dissolved in acidic electrolyte creating the In-deficient layer and then been electrochemically reduced back onto the electrode's surface. These nodes are not Pt, which was found only at the Pt disk. P appears nearly homogeneous with decreased detection in the interlayer. High concentrations of P observed in the Pt disk region may be a result of higher-order scattering events emitting X-rays from the neighboring region, the interlayer, as well as possible interface "smearing" during FIB cross-sectioning. The Pt Lα peak and P Kα peak were used to identify Pt and P, respectively, to avoid misidentification of Pt by peak overlap with P Kα. However, the Pt M and P Kα peak overlap and the uncertainty in deconvolving the peaks (i.e., Pt M identified as P Kα) may contribute to the higher-than-expected apparent concentration of P in the Pt region.

The low oxygen detection was attributed to its small atomic number yielding low detection sensitivity. The higher concentration of oxygen observed in the Pt disk region was thus attributed to electron scattering into the interlayer and not Pt oxide. For more-accurate surface-chemical analysis

https://doi.org/10.1021/acsenergylett.1c02590
ACS Energy Lett. 2022, 7, 541−549

unaffected by these possible artifacts, XPS was used to identity the composition of the amorphous surface oxides and other surface species (Figure 5b).

Outlook. Pt prepared on pretreated p-InP surfaces should yield an ohmic/nonselective junction based on simple Schottky-contact models, and this is observed experimentally (Figures 2b and 3c). The H_2O_2/HCl pretreatment removes surface oxides (Figures 1f,g and S1a,b), resulting in a more-pristine Pt/p-InP interface which was nonselective and ohmic in dry $J-V$ curves. The substantial presence of In_2O_3 and $In_x(PO_y)_z$ by XPS, however, corresponded to rectifying $J-V$ curves. In_2O_3 may exist in the periphery, giving rise to the pinch-off effect, which is evident from the size-dependent photovoltages found for EBL Pt/p-InP. However, no size dependence is observed in V_{oc} after dark and light CV analysis (Figure 4b). Further oxidation underneath the Pt by either undercutting or oxygen diffusion through the Pt film would increase the barrier (V_{oc}) and eventually diminish the pinch-off effect due to heterojunction formation.

After driving the HER, the photocurrent and V_{oc} were observed to decrease (Figure S10c,e). Other groups have shown similar behavior and attributed it to the removal of a surface oxide.[1,6] Allowing the surface to rest at V_{oc} restores the photovoltage (Figure S10b,d), presumably due to the regrowth of the oxide under the more-positive rest potential of the system. Changes in the photovoltage might also be affected by hydrogen spill over at Pt nanoparticles.[39] Another important feature is likely the protection of n-type In_2O_3 (that forms the electrical heterojunction with p-InP) from etching by indium phosphates and polyphosphates that are more chemically stable at pH 0 leading to a layered surface-oxide structure.[6,10,24] After photoelectrochemical analysis, nanoscale electrical contacts on p-InP share similar electrical properties as the macroscopic thin-film sample. These experiments thus support the idea that the formation of a dynamic surface oxide, that is slowly dissolving and reforming, is responsible for generating the electron-selective catalyst contacts for precious metals on p-InP and likely also p-$Ga_xIn_{1-x}P$.

InP is one example of a highly efficient absorber used in photoelectrodes which readily form n-type surface oxides.[13,23,40,41] We demonstrated a mechanism by which efficient absorbers may be decorated with the desired catalysts while the absorber's surface becomes carrier-selective by natural oxidation (*i.e.*, without additional thin-film deposition steps). We showed various mechanisms control electron selectivity in different ways and situations. H_2 alloying, the previously proposed mechanism, is not primarily responsible for governing the selectivity in this system. Instead, the surface indium oxide forms an adaptive junction that becomes more electron-selective as the catalyst layer accumulates negative charge, likely due to the reduction (increased electron doping) of the hydrated and porous In oxide.[34] Such adaptive-junction effects have not previously been considered in the context of conducting metal-oxide heterojunctions on III–V semiconductors.

These results are further broadly important for other PEC systems, like $BiVO_4$ and metal sulfides, where vacancy/defect modulation at the semiconductor surface could affect carrier selectivity by modulating the carrier concentration in that region (and hence band bending and conductivity surrounding or under a catalyst contact).[42,43] In this work, we observed the formation of an n-type oxide (likely doped with oxygen vacancies and protonic defects) increasing electron selectivity. Similarly for oxide photoelectrodes, the surface near the electrocatalyst contact could become reduced (e.g., by e^-/H^+ injection) or further oxidized (relative to the bulk, either at surface cations or at bridging or terminal oxo groups), which in turn would increase the electron and hole selectivity, respectively.

Single-particle overall-water-splitting systems, where both hydrogen- and oxygen-evolution reactions occur at spatially separated contacts on the same particle, are likely also influenced by related phenomena. These contacts, for example, might become more selective for their appropriate reaction when the surface is reduced or further oxidized either under or around the catalyst/semiconductor interface.[25,26] The presence of H_2 alloying also might similarly increase the electron selectivity for the metal HER catalyst in single-particle photocatalysts. Single-particle systems which are decorated with nanoparticle electrocatalysts would also be subject to the pinch-off effect if a peripheral material forms a larger barrier than at the catalyst/semiconductor junction alone. Transformations in the surrounding surface (shown in this work by the growth of indium oxide) or intentional catalyst coatings employed in core–shell architectures might provide the peripheral material required for pinch-off-enhanced selectivity. As a specific example, an increase in electron selectivity of HER catalysis during operation on single-particle systems may in fact be important to enhance carrier separation and contribute to the high external quantum efficiency observed on optimized catalyst-decorated $SrTiO_3$.[25] In sum, the mechanisms detailed in this work may provide further routes to enhance performance—or in fact already play a significant role in efficient carrier separation—on a variety of overall water splitting particles, photoanodes, and photocathodes.

■ ASSOCIATED CONTENT

Supporting Information

The Supporting Information is available free of charge at https://pubs.acs.org/doi/10.1021/acsenergylett.1c02590.

Details of experimental methods; supporting figures; and additional XPS, heterostructure, and transport discussions (PDF)

■ AUTHOR INFORMATION

Corresponding Author

Shannon W. Boettcher − *Department of Chemistry and Biochemistry, University of Oregon, Eugene, Oregon 97403, United States;* orcid.org/0000-0001-8971-9123; Email: swb@uoregon.edu

Authors

Aaron J. Kaufman − *Department of Chemistry and Biochemistry, University of Oregon, Eugene, Oregon 97403, United States*

Raina A. Krivina − *Department of Chemistry and Biochemistry, University of Oregon, Eugene, Oregon 97403, United States*

Meikun Shen − *Department of Chemistry and Biochemistry, University of Oregon, Eugene, Oregon 97403, United States;* orcid.org/0000-0001-8100-4115

Complete contact information is available at: https://pubs.acs.org/10.1021/acsenergylett.1c02590

Notes

The authors declare no competing financial interest.

■ ACKNOWLEDGMENTS

This work was funded by the Department of Energy, Basic Energy Sciences award no. DE-SC0014279. A.J.K. and S.W.B. conceived the experiments and led the project. R.A.K. collected, processed, and consulted on XPS data analysis. TEM images were collected by Peter Eschbach, Facility Director at Oregon State University Electron Microscopy Facility. A.J.K. conducted all other experiments. A.J.K and S.W.B. analyzed the data and wrote the manuscript with input from all authors.

■ REFERENCES

(1) Heller, A.; Aharon-Shalom, E.; Bonner, W. A.; Miller, B. Hydrogen-Evolving Semiconductor Photocathodes: Nature of the Junction and Function of the Platinum Group Metal Catalyst. *J. Am. Chem. Soc.* **1982**, *104* (25), 6942−6948.

(2) Heller, A.; Vadimsky, R. G. Efficient Solar to Chemical Conversion: 12% Efficient Photoassisted Electrolysis in the [p-Type InP(Ru)]/HCl-KCl/Pt(Rh) Cell. *Phys. Rev. Lett.* **1981**, *46* (17), 1153−1156.

(3) Aspnes, D. E.; Heller, A. Photoelectrochemical Hydrogen Evolution and Water Photolyzing Semiconductor Suspensions: Properties of Platinum Group Metal Catalyst-Semiconductor Contacts in Air and in Hydrogen. *J. Phys. Chem.* **1983**, *87* (24), 4919−4929.

(4) Trasatti, S. Work Function, Electronegativity, and Electrochemical Behaviour of Metals: III. Electrolytic Hydrogen Evolution in Acid Solutions. *J. Electroanal. Chem. Interface Electrochem.* **1972**, *39* (1), 163−184.

(5) Sze, S. M.; Ng, K. K. *Physics of Semiconductor Devices*; John Wiley & Sons, Inc.: Hoboken, NJ, 2006. DOI: 10.1002/0470068329.

(6) Lewerenz, H. J. Semiconductor Surface Transformations for Photoelectrochemical Energy Conversion. *J. Electrochem. Soc.* **2014**, *161* (13), H3117.

(7) Lee, M. H.; Takei, K.; Zhang, J.; Kapadia, R.; Zheng, M.; Chen, Y.-Z.; Nah, J.; Matthews, T. S.; Chueh, Y.-L.; Ager, J. W.; Javey, A. P-Type InP Nanopillar Photocathodes for Efficient Solar-Driven Hydrogen Production. *Angew. Chem., Int. Ed.* **2012**, *51* (43), 10760−10764.

(8) Nunez, P.; Cabán-Acevedo, M.; Yu, W.; Richter, M. H.; Kennedy, K.; Villarino, A. M.; Brunschwig, B. S.; Lewis, N. S. Origin of the Electrical Barrier in Electrolessly Deposited Platinum Nanoparticles on P-Si Surfaces. *J. Phys. Chem. C* **2021**, *125* (32), 17660−17670.

(9) van Dorp, D. H.; Cuypers, D.; Arnauts, S.; Moussa, A.; Rodriguez, L.; De Gendt, S. Wet Chemical Etching of InP for Cleaning Applications: II. Oxide Removal. *ECS J. Solid State Sci. Technol.* **2013**, *2* (4), P190.

(10) Faur, M.; Faur, M.; Jayne, D. T.; Goradia, M.; Goradia, C. XPS Investigation of Anodic Oxides Grown on P-Type InP. *Surf. Interface Anal.* **1990**, *15* (11), 641−650.

(11) Hollinger, G.; Bergignat, E.; Joseph, J.; Robach, Y. On the Nature of Oxides on InP Surfaces. *J. Vac. Sci. Technol. A* **1985**, *3* (6), 2082−2088.

(12) Hofmann, A.; Streubel, P.; Meisel, A. XPS Investigation of Oxide Films on InP(100). *Surf. Interface Anal.* **1988**, *12* (5), 315−319.

(13) Hussey, R. J.; Sproule, G. I.; McCaffrey, J. P.; Graham, M. J. Characterization of Oxides Formed on InP, InGaAs, InAlAs, and InGaAs/InAlAs Heterostructures at 300−500°C. *Oxid. Met.* **2002**, *57* (5), 427−447.

(14) Pakes, A.; Skeldon, P.; Thompson, G. E.; Hussey, R. J.; Moisa, S.; Sproule, G. I.; Landheer, D.; Graham, M. J. Composition and Growth of Anodic and Thermal Oxides on InP and GaAs. *Surf. Interface Anal.* **2002**, *34* (1), 481−484.

(15) Goryachev, A.; Gao, L.; van Veldhoven, R. P. J.; Haverkort, J. E. M.; Hofmann, J. P.; Hensen, E. J. M. On the Origin of the Photocurrent of Electrochemically Passivated P-InP(100) Photoelectrodes. *Phys. Chem. Chem. Phys.* **2018**, *20* (20), 14242−14250.

(16) Wurfel, U.; Cuevas, A.; Wurfel, P. Charge Carrier Separation in Solar Cells. *IEEE J. Photovoltaics* **2015**, *5* (1), 461−469.

(17) Leibovitch, M.; Kronik, L.; Fefer, E.; Korobov, V.; Shapira, Y. Constructing Band Diagrams of Semiconductor Heterojunctions. *Appl. Phys. Lett.* **1995**, *66* (4), 457−459.

(18) Laskowski, F. A. L.; Oener, S. Z.; Nellist, M. R.; Gordon, A. M.; Bain, D. C.; Fehrs, J. L.; Boettcher, S. W. Nanoscale Semiconductor/Catalyst Interfaces in Photoelectrochemistry. *Nat. Mater.* **2020**, *19* (1), 69−76.

(19) Tung, R. T. The Physics and Chemistry of the Schottky Barrier Height. *Appl. Phys. Rev.* **2014**, *1* (1), 011304.

(20) Tung, R. T. Electron Transport at Metal-Semiconductor Interfaces: General Theory. *Phys. Rev. B* **1992**, *45* (23), 13509−13523.

(21) Tung, R. T. Electron Transport of Inhomogeneous Schottky Barriers. *Appl. Phys. Lett.* **1991**, *58* (24), 2821−2823.

(22) Khaselev, O.; Turner, J. A. A Monolithic Photovoltaic-Photoelectrochemical Device for Hydrogen Production via Water Splitting. *Science* **1998**, *280* (5362), 425−427.

(23) Young, J. L.; Steiner, M. A.; Döscher, H.; France, R. M.; Turner, J. A.; Deutsch, T. G. Direct Solar-to-Hydrogen Conversion via Inverted Metamorphic Multi-Junction Semiconductor Architectures. *Nat. Energy* **2017**, *2* (4), 1−8.

(24) Yu, W.; Richter, M. H.; Buabthong, P.; Moreno-Hernandez, I. A.; Read, C. G.; Simonoff, E.; Brunschwig, B. S.; Lewis, N. S. Investigations of the Stability of Etched or Platinized P-InP(100) Photocathodes for Solar-Driven Hydrogen Evolution in Acidic or Alkaline Aqueous Electrolytes. *Energy Environ. Sci.* **2021**, *14*, 6007.

(25) Takata, T.; Jiang, J.; Sakata, Y.; Nakabayashi, M.; Shibata, N.; Nandal, V.; Seki, K.; Hisatomi, T.; Domen, K. Photocatalytic Water Splitting with a Quantum Efficiency of Almost Unity. *Nature* **2020**, *581* (7809), 411−414.

(26) Nishiyama, H.; Yamada, T.; Nakabayashi, M.; Maehara, Y.; Yamaguchi, M.; Kuromiya, Y.; Nagatsuma, Y.; Tokudome, H.; Akiyama, S.; Watanabe, T.; Narushima, R.; Okunaka, S.; Shibata, N.; Takata, T.; Hisatomi, T.; Domen, K. Photocatalytic Solar Hydrogen Production from Water on a 100-m2 Scale. *Nature* **2021**, *598* (7880), 304−307.

(27) Roe, E. T.; Egelhofer, K. E.; Lonergan, M. C. Limits of Contact Selectivity/Recombination on the Open-Circuit Voltage of a Photovoltaic. *ACS Appl. Energy Mater.* **2018**, *1* (3), 1037−1046.

(28) Oener, S. Z.; Cavalli, A.; Sun, H.; Haverkort, J. E. M.; Bakkers, E. P. A. M.; Garnett, E. C. Charge Carrier-Selective Contacts for Nanowire Solar Cells. *Nat. Commun.* **2018**, *9* (1), 3248.

(29) Lundström, I.; DiStefano, T. Hydrogen Induced Interfacial Polarization at Pd-SiO2 Interfaces. *Surf. Sci.* **1976**, *59* (1), 23−32.

(30) Armgarth, M.; Söderberg, D.; Lundström, I. Palladium and Platinum Gate Metal-Oxide-Semiconductor Capacitors in Hydrogen and Oxygen Mixtures. *Appl. Phys. Lett.* **1982**, *41* (7), 654−655.

(31) Lundström, I. Hydrogen Sensitive MOS-Structures. *Sens. Actuator* **1981**, *1*, 403−426.

(32) Nellist, M. R.; Laskowski, F. A. L.; Lin, F.; Mills, T. J.; Boettcher, S. W. Semiconductor−Electrocatalyst Interfaces: Theory, Experiment, and Applications in Photoelectrochemical Water Splitting. *Acc. Chem. Res.* **2016**, *49* (4), 733−740.

(33) Laskowski, F. A. L.; Nellist, M. R.; Venkatkarthick, R.; Boettcher, S. W. Junction Behavior of N-Si Photoanodes Protected by Thin Ni Elucidated from Dual Working Electrode Photoelectrochemistry. *Energy Environ. Sci.* **2017**, *10* (2), 570−579.

(34) Van de Walle, C. G.; Neugebauer, J. Universal Alignment of Hydrogen Levels in Semiconductors, Insulators and Solutions. *Nature* **2003**, *423* (6940), 626−628.

(35) Gu, Z.; Zhang, L.; Wen, B.; An, X.; Lan, H.; Liu, L.-M.; Chen, T.; Zhang, J.; Cao, X.; Tang, J.; Liu, H.; Qu, J. Efficient Design

Principle for Interfacial Charge Separation in Hydrogen-Intercalated Nonstoichiometric Oxides. *Nano Energy* **2018**, *53*, 887−897.
(36) Meléndez, J. J.; Wierzbowska, M. In2O3 Doped with Hydrogen: Electronic Structure and Optical Properties from the Pseudopotential Self-Interaction Corrected Density Functional Theory and the Random Phase Approximation. *J. Phys. Chem. C* **2016**, *120* (7), 4007−4015.
(37) Kumar, M.; Chatterjee, R.; Milikisiyants, S.; Kanjilal, A.; Voelskow, M.; Grambole, D.; Lakshmi, K. V.; Singh, J. P. Investigating the Role of Hydrogen in Indium Oxide Tubular Nanostructures as a Donor or Oxygen Vacancy Passivation Center. *Appl. Phys. Lett.* **2009**, *95* (1), 013102.
(38) King, P. D. C.; Lichti, R. L.; Celebi, Y. G.; Gil, J. M.; Vilão, R. C.; Alberto, H. V.; Piroto Duarte, J.; Payne, D. J.; Egdell, R. G.; McKenzie, I.; McConville, C. F.; Cox, S. F. J.; Veal, T. D. Shallow Donor State of Hydrogen in In_2O_3 and SnO_2: Implications for Conductivity in Transparent Conducting Oxides. *Phys. Rev. B* **2009**, *80* (8), 081201.
(39) Karim, W.; Spreafico, C.; Kleibert, A.; Gobrecht, J.; VandeVondele, J.; Ekinci, Y.; van Bokhoven, J. A. Catalyst Support Effects on Hydrogen Spillover. *Nature* **2017**, *541* (7635), 68−71.
(40) Lin, J.; Wang, W.; Li, G. Modulating Surface/Interface Structure of Emerging InGaN Nanowires for Efficient Photoelectrochemical Water Splitting. *Adv. Funct. Mater.* **2020**, *30* (52), 2005677.
(41) Kao, Y.-C.; Chou, H.-M.; Hsu, S.-C.; Lin, A.; Lin, C.-C.; Shih, Z.-H.; Chang, C.-L.; Hong, H.-F.; Horng, R.-H. Performance Comparison of III−V//Si and III−V//InGaAs Multi-Junction Solar Cells Fabricated by the Combination of Mechanical Stacking and Wire Bonding. *SCi. Rep.* **2019**, *9* (1), 4308.
(42) Filippone, F.; Mattioli, G.; Polimeni, A.; Felici, M.; Bonapasta, A. A. Opposite Hydrogen Behaviors in GaAsN and InAsN Alloys: Band Gap Opening Versus Donor Doping. *J. Phys. Chem. C* **2020**, *124* (35), 19240−19251.
(43) Cooper, J. K.; Scott, S. B.; Ling, Y.; Yang, J.; Hao, S.; Li, Y.; Toma, F. M.; Stutzmann, M.; Lakshmi, K. V.; Sharp, I. D. Role of Hydrogen in Defining the N-Type Character of BiVO4 Photoanodes. *Chem. Mater.* **2016**, *28* (16), 5761−5771.

https://doi.org/10.1021/acsenergylett.1c02590
ACS Energy Lett. 2022, 7, 541−549